Fluid Flow and Convective Heat Transfer Analysis on a Rotor of Wind Turbine Alternator with an Impinging Jet

Chadia Haidar*‡, Rachid Boutarfa**, Souad Harmand***

*Department of Mechanical Engineering, Faculty of Science and Technology, BP: 577, Route de Casa -, Settat, MOROCCO

** Department of Mechanical Engineering, Faculty of Science and Technology, BP: 577, Route de Casa -, Settat, MOROCCO

*** F-59000 Lille UVHC, TEMPO-DF2T, University Polytechnic of Hauts-de-France, Famars-59313 Valenciennes, France

(c.haidar@uhp.ac.ma, boutarfarachid@yahoo.fr, Souad.Harmand@univ-valenciennes.fr)

‡ Corresponding Author; Chadia Haidar, Tel: +212 606 18 12 35, c.haidar@uhp.ac.ma

Received: 03.05.2019 Accepted:04.06.2019

Abstract- This work presents a numerical and experimental study of convection heat transfer in the unconfined air gap of a discoidal technology rotor-stator system. In particular, the rotor is cooled here by an eccentric air jet impingement. The cavity is characterized by a dimensionless spacing G = 0.02 and a low aspect ratio for the jet H/D= 0.25. the rotational Reynolds numbers from $Re_\omega = 2.38\times10^5$ to 5.44×10^5 and the jet Reynolds number between 16.5×10^3 and 49.5×10^3 are used. The experimental technique is based on using infrared thermography to access the rotor surface temperature measurement, and on the numerical resolution of the energy equation at steady state to evaluate the local convective coefficient. The numerical study is based on the turbulence model RSM (Reynolds Stress Model). The results of this study are described in terms of radial distributions of the mean velocity components, Reynolds stress tensor components and corresponding local and mean Nusselt numbers. Three flow regions have been identified: a region dominated by the air jet, a mixed zone at low radii and a zone dominated by outward rotation. A good agreement between the two approaches has been obtained, which confirms our choice of numerical turbulence model.

Keywords Alternator, Rotor-stator system, Impingement jet, Convective heat transfer, RSM turbulence model, Infrared thermography.

1. Introduction

Nowadays, the concept of sustainable development requires an increase in the production of so-called "clean" energy. Indeed, in order to better preserve the planet's natural resources [1, 2,3], the processes used to transform energy must be optimized or be a different nature [4]. For this reason, wind turbines [5,6] have developed in recent years, since they convert mechanical energy linked to the wind into electrical energy [7], without producing greenhouse gases such as CO_2. The optimization study of these wind turbines and the generators embarked on them has highlighted the so-called "discoidal" technology. Indeed, this technology, which puts a rotating disk (rotor) against a fixed disk (stator), allows obtaining a high power even at low rotational velocities. However, the major disadvantage is that the air flow induced by the generator's rotation is not always adequate for optimum cooling of the installation.

Heat transfer on a rotating disk in rest air was studied by Goldstein [8] , Cobb and Saunders [9] and later by Dorfman [10]. Dorfman [10] proposed many correlations for local and mean Nusselt numbers, considering the radial temperature profile on the disk surface.

The heat transfers on a single rotating disk with an air jet have been done by Angioletti [11]. This author has shown that heat transfers are significant near the impinging jet on the disk. Indeed, the jet renews the air more quickly and disrupts the boundary layer that is created by the rotation of the disk, because vortices appear at the jet's outlet. The influence of the jet diameter (D), the jet Reynolds number ($\mathrm{Re_j}$) and the distance between the jet outlet and the impacted surface H/D

were highlighted by Chen [12] and Owen [13]. Popiel [14] distinguished three areas on the disk surface with an axial jet: an area near the impinging point where the jet's influence is preponderant on heat transfers, an area outside the disk where rotation is preponderant and a mixed area, located between the two previous one.

In the case of rotor-stator systems, several types of configurations exist, including partially or completely closed, which are widely documented, and open configurations are not quite well documented. When a fixed disk is placed opposite a rotating disk, the axial suction is replaced by a centripetal flow on the stator. A Batchelor [15] type flow can be observed with a rotating fluid core, in which radial velocities are zero. It is also possible to have a Stewartson [16] type flow without a rotating fluid core. It is also necessary to distinguish laminar from turbulent regimes. The separations between different regimes are synthesized by Daily and Nece [17] according to a rotational Reynolds number Re_ω and spacing between both disks G. A similar classification for air gaps with an air jet is proposed by Owen [13].

Pellé [18] experimentally studied heat transfer in the case of an unconfined rotor-stator system with an axisymmetric air jet for different dimensionless spacings ($0.01 £ G £ 0.16$). He showed that the rotating disk surface was divided into three zones where the influence of jet or rotation on heat transfer is preponderant and a mixed zone. The three zones do not necessarily appear simultaneously on the disk surface. They depend in particular on the flow rate injected and the rotational velocity. This author showed that for higher inter-disk spacing (G = 0.16), heat transfer tends towards a single disk and proposed a correlation giving the mean Nusselt number $\overline{Nu} = 0.06¥ Re_j^{0.25}¥ Re_w^{0.5}$ for $Re_\omega \geq 1.29\times10^5$ and Re_j between $8.3¥ 10^3$ and $41.6¥ 10^3$.

The flow structure in a rotor-stator configuration with an axial impinging jet was experimentally studied by Nguyen [19] for a dimensionless spacing of G = 0.02. This author showed that, for small radii and near the impinging point, the rotation effects on the flow structure are negligible compared to those of the jet. On the other hand, for large radii, the flow structure is dominated by rotating effects and the flow becomes centrifugal on the rotor surface.

Poncet [20] numerically studied the influence of the rotation coupling and the air flow on the convective transfer on a rotating disk placed facing a fixed disk. The turbulence models tested are k -ω SST and RSM. The author noted that the model k -ω SST tends to overestimate the flow characteristics in the impingement region. However, the results obtained with the RSM model are in good agreement with experimental results [19]. The author also observes the presence of two peaks in heat transfer. Lytle and Webb [21] have shown that this first peak is $r/2R_j = 0.5$ in while the second is given by the following relationship [21]:

$$\frac{r}{2R_j} = 0.188\times Re_j^{0.241}\times\left(\frac{H}{2R_j}\right)^{0.224} \quad (1)$$

The most common configurations encountered are those of low inter-disk space, which leads to poor cooling. The addition of an air jet impingement of velocity U_j and diameter D is an interesting solution to overcome this problem. Nevertheless, we have not reported in the literature a study on a configuration similar the one we have in which an eccentric jet impingement, rotation and opening of the air gap to the outside are present. The only studies on convective transfer between coaxial disks that are close to our configuration have been carried out in the case of rotor-stator systems with axial jet. This study then proposes to present the global flow structure and compare it with the convective heat transfers on the rotor.

2. Experimental Study

2.1 Experimental set-up

Figure 1 shows the main elements of the experimental bench used. The rotor has a radius R = 0.31m and its rotation velocity can be varied between 450 and 850 rpm using a frequency regulator. The rotor is composed of a highly conductive aluminum disk $(l = 200\,W/mK)$, on which e=2.5 mm of zircon, thermal conductivity insulating material $(l_{zir} = 0.7\,W/mK)$, has been deposed by plasma projection. It is then heated from its back surface using infrared emitters with a total power of 12 kW and cooled on the surface turned towards the jet. The stator is placed facing the rotor at a distance H=6.5mm for a dimensionless spacing G=0.02. The stator used is made of aluminum and has the same diameter as the rotor. It is pierced by an eccentric opening of diameter $D = 26mm$ to ensure the passage of a long, cylindrical pipe connected to a centrifugal blower, which is used to impose an eccentric air jet. The mean jet velocity U_j is between 10 and 30 m/s, corresponding respectively to the jet Reynolds numbers $Re_j = 16.5\times10^3$ to $49.5¥ 10^3$.

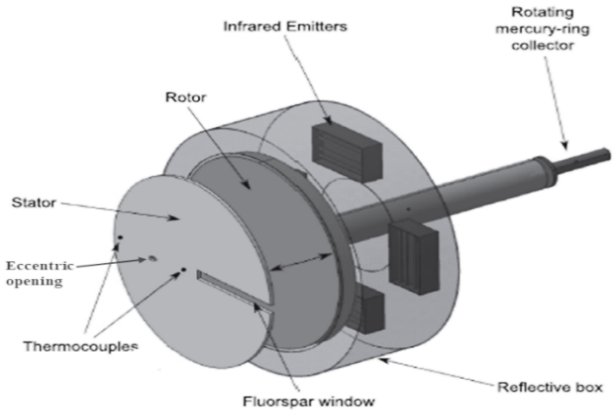

Fig. 1. Experimental set-up

2.2. Local Nusselt numbers calculation

To access the local convective exchange coefficient h and the local Nusselt number Nu, it is necessary to determine the

parietal flux on the rotor surface. Solving the Laplace equation within the insulation allows access to it.

$$\frac{\partial^2 T}{\partial r^2}+\frac{1}{r}\times\frac{\partial T}{\partial r}+\frac{\partial^2 T}{\partial z^2}=0 \quad (2)$$

A zircon mesh is performed as well as a resolution by the difference-finite method. The bondary conditions are, on the one hand, the temperature mesured via infrared thermography on the zircon insulating surface subjected to the air flow $T(r,z=0)$, and on the other hand, the interface aluminum/zircon temperature $T(r,z=e)$ given via the thermocouples.

The conductive heat flux density j_{cd} in the insulation at z=0 is calculated by [14,18] :

$$\varphi_{cd}=\varphi_{cv}+\varphi_{ray}=\lambda_{zir}\times\left(\frac{\partial T_{(r,z)}}{\partial z}\right)_{z=0} \quad (3)$$

The radiative heat flux φ_{ray} exchanged between two parallel disks is calculated by [14,18]:

$$\varphi_{ray}=\sigma\frac{F\varepsilon_r\varepsilon_S}{1-F^2(1-\varepsilon_r)(1-\varepsilon_s)}\left(T(r,z=0)^4-T_{stator}^4\right) \quad (4)$$

With F is a view factor as a function of dimensionless spacing G, it is calculated by Ritoux [23]:

$$F=1+\frac{G^2}{2}-\sqrt{\frac{G^4}{4}+G^2} \quad (5)$$

The heat transfer exchanged by convection φ_{cv} can be written as follows [14,18] :

$$\varphi_{cv}=h\times(T_{(r,z)}-T_\infty) \quad (6)$$

So, these equations provide access to the local convective exchange coefficient (h) and the local Nusselt number ($Nu=\frac{h¥ r}{l_{air}}$) [14,18] :

$$h=\frac{\lambda_{zir}\left(\frac{\partial T(r)}{\partial z}\right)_{z=0}-\sigma\frac{F\varepsilon_r\varepsilon_s}{1-F^2(1-\varepsilon_r)(1-\varepsilon_s)}\left(T(r,z=0)^4-T_{stator}^4\right)}{T(r,z=0)-T_\infty} \quad (7)$$

$$Nu=\frac{\lambda_{zir}\left(\frac{\partial T(r)}{\partial z}\right)_{z=0}-\sigma\frac{F\varepsilon_r\varepsilon_s}{1-F^2(1-\varepsilon_r)(1-\varepsilon_s)}\left(T(r,z=0)^4-T_{stator}^4\right)}{T(r,z=0)-T_\infty}\times\frac{r}{\lambda_{air}} \quad (8)$$

The mean Nusselt number defined by $\overline{Nu}=\frac{\bar{h}¥ r}{l_{air}}$ is given as follows [14,18,20]:

$$\overline{Nu}=\frac{2}{R}\times\frac{\int_0^r Nu\times(T_{(r,z=0)}-T_\infty)\,dr}{T_{(r,z=0)}-T_\infty} \quad (9)$$

2.3. Measurement techniques

2.3.1. Rotor surface temperature measurement

The rotor surface temperatures are obtained from the thermal levels measured by an SC 7000 infrared camera. To favor the thermal emission of the rotor over parasitic flows, the rotating disk is covered with black paint, considered grey and diffusing in emission and reflections. The emissivity of this surface is estimated by calibration at $e_r=0.937\pm0.01$. In a measurement situation, the camera gives the thermal level I_r which can be expressed as follows [22]:

$$I_r=\tau_f\times\tau\times J_r+(1-\tau)\times I(T_\infty)+\tau\times\tau_f^2\times(1-\acute{U}_r)\times I_{env} \quad (10)$$

The rotor radiosity J_r is interpreted as what is emitted by the rotor added to all reflections from other system surfaces. Thus, the camera receives the radiosity of the rotor attenuated by fluorspar and the atmosphere, to which are added an atmospheric term $I(T_\infty)$ and an environmental term I_{env}. The term $I(T_\infty)$ is measured directly via infrared thermography using a crumpled aluminum film placed near the disk. The term is obtained using the calibration law because the atmospheric temperature is easily obtained using a thermocouple. To solve a radiosity system, we consider the air gap as a closed system. The limits are the rotor, stator, fluorine window, and air crown. All limits are considered grey surfaces whose rotor and stator temperatures are measured using the thermocouple and considered isothermal. The evaluation of the disk surface temperature depends on the calibration law, the emissivity of the black paint covering the rotor, the air temperature, and its transmission coefficient. It also depends on additional parameters such as the emissivity of the grey paint ε_s covering the stator and the transmission coefficient τ_f of the fluorine window, which is provided by the supplier as being $\tau_f=0.95\pm0.01$. The temperature uncertainty estimates T gives ΔT=0.9K for our temperature range $323<T<371\ K$.

2.3.2.Temperature measurement at the aluminum/zircon interface

They are measured using two T-type thermocouples that are placed at two different radii (r=150 mm, r=300 mm) at the interface between aluminum and zircon. The wires pass through the rotation shaft to a rotating four-channel mercury annular collector and are connected to the central acquisition system. The absolute temperature measurement error at the interface between aluminum and zircon is estimated at $\Delta T=\pm0.3K$.

2.3.3. Atmospheric temperature measurement

The reference air temperature T_∞ is measured using a T-type thermocouple placed at a distance of 1000 mm from the disk surface. The absolute error is estimated at $\Delta T_\infty = \pm 0.3K$.

2.3.4.Stator temperature measurement

Two type T thermocouples are positioned on the stator surface that is contacting with the air gap: one at r=0.05m and the other at r=0.3m. They are directly linked to the acquisition system. These thermocouples are used to calculate the radiative heat flux exchanged by two disks and the radiosity of the rotor. The absolute error on the stator temperature is estimated at ±0,3 K.

3. Numerical Simulation

3.1. Geometric model

The rotor-stator cavity corresponds to the experimental set-up considered is shown in Figure 2, by modeling two disks having the same radius (R=0.31m), one rotating (the rotor) and the other is stationary (the stator). The geometric configuration is open. The geometric characteristics of the rotor and stator are the same as those described in section 2.1. The air flows through the inlet cylindrical tube of the radius $R_j = 13mm$ and length $H' = 0.75\text{m}$ before impinging on the rotating disk. The spacing between two disks is set to $H = 6.5\text{mm}$ such that $G = H/R = 0.02$. Hydrodynamic flow and forced convection heat transfer are mainly influenced by the jet Reynolds number Re_j and rotational Reynold number Re_ω defined respectively as:

$$Re_\omega = R\omega^2/\vartheta_{air} \quad Re_j = U_j D/\vartheta_{air}$$

Where ϑ_{air} is the kinematic viscosity of air.

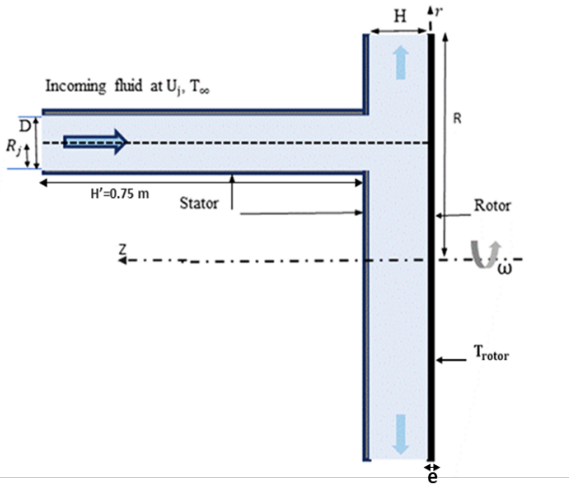

Fig 2. Rotor-stator system configuration.

The small spacing between two disks of the system imposes a very fine mesh in the air gap. In fact, to perfectly represent phenomena occurring in the boundary layers, an adequate refinement is imposed near the walls so that the first parietal mesh respects the condition $Y^+ = 1$. This implies a different mesh size when the jet and rotational velocities change. A boundary layer of 10 meshes is modelled at the edges of each disk. The numerical procedure is based on the finite-volume method used with staggered grids for the mean velocity components. In order to describe the local thermal characteristics, a square and polyhedral regular mesh is generated in the study field. The independence of the solution vis-à-vis the mesh size is studied and leads to the use of mesh size having a cell number equal to 3×10^6 cells. The effect of mesh refinement on the computations is presented by the evolution of the mean Nusselt number as a function of the cell number for $Re_j = 33\times10^3$ and $Re_\omega = 2.38\times10^5$ (tab.1). The mean Nusselt values increase by increasing the cell number. From a cell number of 3×10^6, the mean Nusselt values remain constant. This configuration is considered as the optimal mesh where the results are not dependent on the mesh.

Table 1. Study of mesh sensitivity

Cell number	2×10^6	2.5×10^6	3×10^6	3.5×10^6	4×10^6
Mean Nusselt number	350	375	416	416	416

3.2. Turbulence model

The ANSYS Fluent [25] computation code proposes different closure models to describe turbulent aspect in the flow. We chose RSM turbulence model (Reynolds Stress Model), presented here, which provides a detailed description of the turbulent field throughout the domain, including near the walls, and has the advantage of not adding a turbulence viscosity hypothesis. The Reynolds stress transport equations are written [26]:

$$\underbrace{\frac{\partial}{\partial x_k}\left(\rho U_k \overline{u_i u_j}\right)}_{1} = \underbrace{-\frac{\partial}{\partial x_k}\left[\rho\overline{u_i u_j u_k} + \overline{p\left(\delta_{kj}u_i + \delta_{ik}u_j\right)}\right]}_{2} + \underbrace{\frac{\partial}{\partial x_k}\left[\mu\frac{\partial}{\partial x_k}\left(\overline{u_i u_j}\right)\right]}_{3} - \underbrace{\left[\overline{u_i u_k}\frac{\partial U_j}{\partial x_k} + u_j u_k \frac{\partial U_i}{\partial x_k}\right]}_{4} + \underbrace{\overline{p\left(\frac{\partial u_i}{\partial x_j} + \frac{\partial u_j}{\partial x_i}\right)}}_{5} - \underbrace{2\mu\overline{\frac{\partial u_i}{\partial x_k}\frac{\partial u_k}{\partial x_k}}}_{6} \quad (11)$$

Where 1 , 2, 3,4,5 and 6 simultaneously denote the following terms: Turbulent diffusion ($D_{T,ij}$), molecular diffusion ($D_{L,ij}$

), production (P_{ij}), pressure-strain correlation term (Φ_{ij}) and dissipation term ε_{ij} .

The pressure-strain correlation equation is written:

$$\phi_{ij} = \phi_{ij,1} + \phi_{ij,2} + \phi_{ij,\omega} \tag{11}$$

The first term $\phi_{ij,1}$ is a non-linear one called "slow".

$$\phi_{ij,1} = -C_1 \rho \frac{\varepsilon}{k}\left[\overline{u_i u_j} - \frac{2}{3}\delta_{ij}k\right] \tag{12}$$

The second term $\phi_{ij,2}$ of the pressure-strain correlation represents the linear part (rapid term).

$$\phi_{ij,2} = -C_2\left[\left(P_{ij} + C_{ij}\right) - \frac{2}{3}\delta_{ij}(P - C)\right] \tag{14}$$

The $\Phi_{ij}^{(W)}$ is a necessary term in the presence of walls. It is modelled according to the classical form proposed by Gibson and Launder [27] in the following relationship:

$$\begin{aligned}\phi_{ij,\omega} = {} & C_1'' \frac{\varepsilon}{k}\left(\overline{u_k u_m} n_k n_m \delta_{ij} - \frac{3}{2}\overline{u_i u_k} n_j n_k - \frac{3}{2}\overline{u_j u_k} n_i n_k\right)\frac{k^{3/2}}{C_l \varepsilon d} \\ & + C_2''\left(\phi_{km,2} n_k n_m \delta_{ij} - \frac{3}{2}\phi_{ik,2} n_j n_k - \frac{3}{2}\phi_{jk,2} n_i n_k\right)\frac{k^{3/2}}{C_l \varepsilon d}\end{aligned} \tag{15}$$

$$C_1 = \frac{C_\mu^{3/4}}{\kappa} \tag{16}$$

The RSM model constants are presented in the following table:

Table 1.the RSM model constants

C_1	C_2	C	C_1''	C_2''	C_μ
1.8	0.6	0.7179	0.5	0.3	0.09

3.3. Numerical scheme

The Navier Stokes equations, turbulent field transport and energy equations are solved sequentially by using the Gauss-Seidel iterative approach and a SIMPLE algorithm, adapted to solve the pressure-velocity coupling problem to avoid the appearance of a pressure field and an irrational velocity field [28]. The Second order upwind discretization [29] is chosen for solving convective terms except for the pressure correction equation where the PRESTO scheme is used. This scheme provides an improved pressure interpolation in the case of the presence of body forces or a high-pressure fluctuation in swirling flows [29].

3.4. Boundary condition

- At the inlet, a uniform velocity and temperature profile (U_j and $T_.$) is imposed. A turbulence level is also imposed corresponding to a turbulence intensity equal to 5% and a hydraulic diameter equal to 0.026 mm.
- At the walls: $U_r = U_z = R_{ij} = 0$ with $(i, j) = (r, q, z)$, except for the tangential velocity is $U_q = wr$ on the rotor and zero on the stationary walls.
- At the outlet, an "outflow" condition is imposed, which means that the flow rate imposed at the inlet is found at the outlet.

The flowing fluid is air with assumed constant physical properties independent of temperature within the temperature range tested. The air flow enters the cavity with a temperature equal to $T_.$, which is the same temperature imposed at the stator walls. At the walls of the rotating disk, an adherence condition and a uniform T_{rotor} temperature are imposed. The rotor is rotated at an angular velocity ω.

4. Results and Discussion

4.1. The flow structures

The dynamic characteristics analysis of the flow in the air gap between rotor and stator is a crucial factor in understanding the local convective heat transfer phenomena on the rotor for the studied spacing (G = 0.02). Several types of flow structures can be distinguished. A flow with two distinct boundary layers separated by an inviscid rotating core is called a Batchelor flow. If the flow has only one boundary layer and a quasi-zero tangential velocity far from it, it is called Stewartson's flow.

Figure 3 shows the mean velocity fields in the air gap between two disks for different rotational Reynolds numbers ranging from $Re_\omega = 2.38\times10^5$ to 5.44×10^5 and a jet Reynolds number set at $Re_j = 33\times10^3$. The jet center is set at r/R = 0.5. Figure 3a shows that the rotational velocity has no significant effect on the axial velocity field $\overline{U_z}$.

In the impingement jet area, the velocity field $\overline{U_r}$ (figure.3.b) indicates positive and negative over-velocities. These over-velocities characterize the change in flow direction and its containment by the recirculation zone. Two zones can be distinguished: one, with low radii ($\frac{r}{R} \leq 0.5$) where the flow is centripetal and another, for larger radii ($\frac{r}{R} \geq 0.5$) where the flow is centrifugal. For higher rotational Reynolds numbers $Re_\omega = 3.87\times10^5$ and $Re_\omega = 5.44\times10^5$, we observe that for the largest radii ($\frac{r}{R} \geq 0.7$) and near the stator, the radial velocity decreases and becomes negative, which corresponds to a fluid inlet from outside the air gap via the boundary layer the stator. This fluid reentry was also observed by Poncet et al [20] and Nguyen et al [19] in the case of a rotor-stator system with an axial jet.

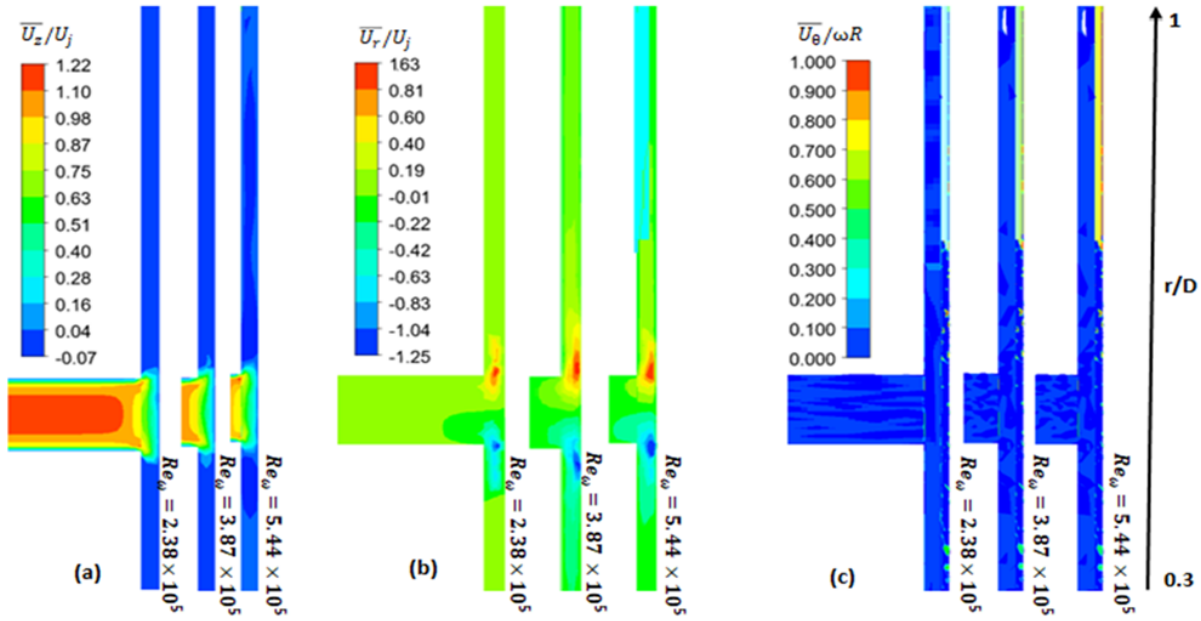

Fig. 3.Mean velocities fields obtained by numerical simulation (a) $\overline{U_z}/U_j$, (b) $\overline{U_r}/U_j$, (c) $\overline{U_q}/wr$ for $Re_j = 33¥10^3$

Figure 3c shows that the fluid is in quasi-solid rotation. As the boundary layer size increases in the radial direction, the flow is gradually dominated by rotation.

Overall, velocities are higher near the rotor than near the stator. The influence of the rotation velocity is greater for the highest radii and also when the jet Reynolds number Re_j is lower. Thus, three areas are distinguished: (i) a centripetal flow throughout the air gap at low radii (ii) a centrifugal flow at high radii near the rotor where the fluid is ejected outwards and (iii) a centripetal flow observed near the stator. This flow is characteristic of a Batchelor type flow in this region of the air gap.

Figure 4 shows the distribution of the radial velocity normalized to jet velocity as a function dimensionless radius r/R. Three positions are considered: near the rotor at Z/H=0.23, a mid-cavity at Z/H = 0.53 and near the stator at Z/H = 0.84.

For the two rotational Reynolds numbers considered $Re_\omega = 3.87\times10^5$ and $Re_\omega = 5.44\times10^5$, there are two velocity peaks at $r/R = 4.7$ and $r/R = 5.7$ due to confinement by the recirculation zone and followed by a sudden decrease in velocity. The radial velocities obtained are confused in this area, which implies that rotation has no influence near the impingement.

Outside the impingement area, differences appear and a negative velocity is observed in Z/H=0.84 for a rotational Reynolds number $Re_\omega = 5.44\times10^5$.This corresponds to a fluid reentry described previously.

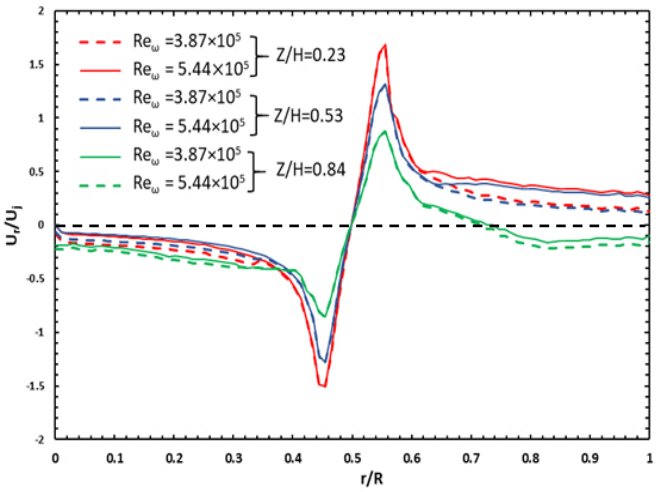

Fig 4.Radial distribution of the mean radial velocity in three different positions: $Z/H = 0.23$, $Z/H = 0.53$, and $Z/H = 0.84$ for two rotational Reynolds numbers $Re_\omega = 3.87\times10^5$ and $Re_\omega = 5.44\times10^5$

4.2. Turbulent field

The radial distribution of the radial and tangential normal components of the Reynolds stress tensor in Z/H = 0.23, 0.53 and 0.84 for two rotational Reynolds numbers are shown in Figure 5. In all cases, peak values for radial component $U_{r,rms}$ (Fig 5.a.b.1) are observed in the impingement zone. They are higher near the rotor at Z/H = 0. 23 and slightly lower when moving towards the stator. The peaks on Reynolds tensions are then reached, which corresponds to the transition from a laminar state to a turbulent state of the boundary layer. A distinct characteristic is achieved for the tangential component $U_{q,rms}$.

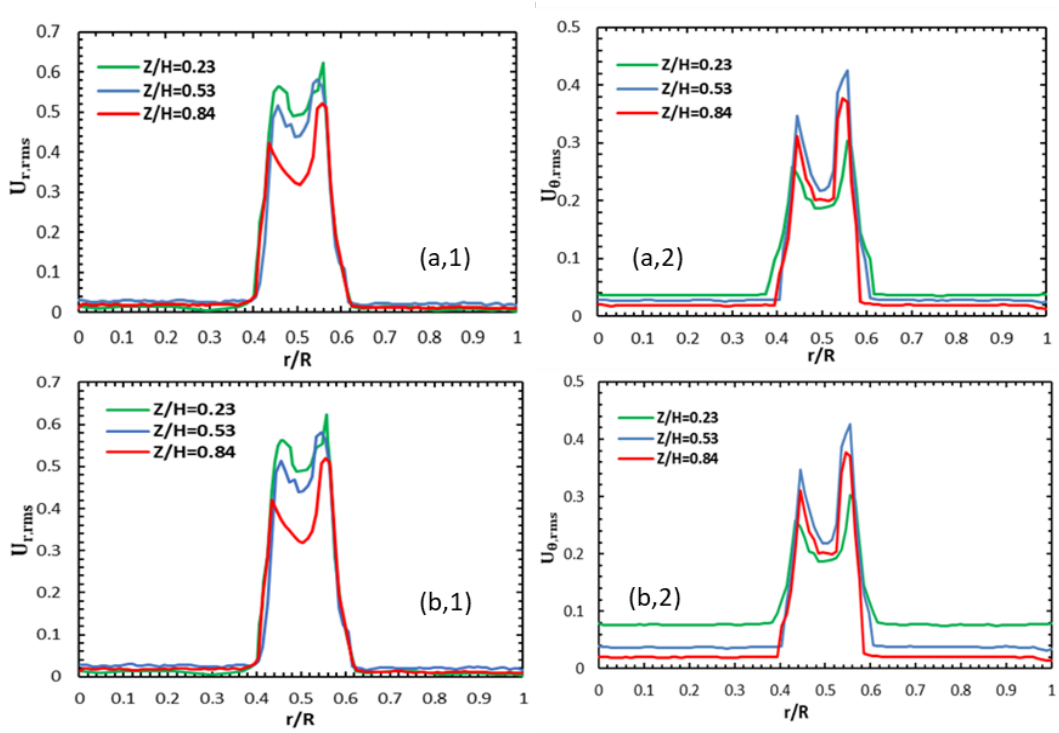

Fig.5. Normal Reynolds stress tensor components ($U_{r,rms}$ left, $U_{q,rms}$ right) obtained for a two rotational Reynolds numbers $Re_\omega = 3.87\times10^5$ (a) and $Re_\omega = 5.44\times10^5$ (b) near the rotor (Z/H = 0.23), at the mid-cavity (Z/H= 0.53) and near the stator (Z/H = 0.84).

A deviation of the tangential component peaks is clearly shown in Figure 5.a.b.2. In the center of the cavity, the peaks of $U_{q,rms}$ are located at r/R=0.46 and r/R = 0.57. They are then at r/R=0.45 and r/R = 0.56 near the stator (Z/H = 0.84) and finally at $r/R = 0.43$ and $r/R = 0.58$ near the rotor (Z/H = 0.23). This radial deviation is attributed to turbulence diffusion in the boundary layer. The rotation has a negligible effect on the radial end tangential components of the Reynolds stress tensor near impingement zone. At larger radii, about $r/R = 0.75$ and for $Re_\omega = 5.44\times10^5$ (fig.b.2), $U_{q,rms}$ increases from the rotor to the stator. So, the rotational influences become dominant.

4.3. Local and mean Nusselt numbers

In order to verify the accuracy of the CFD model proposed in this study, our results from the numerical simulation are compared with heat transfer experiments for $Re_\omega = 2.38\times10^5$ to $Re_\omega = 5.44\times10^5$ and $16.5\times10^3 \le Re_j \le 49.5\times10^3$ (Figure 6).

For a jet Reynolds number fixed $Re_j = 33\times10^3$ (Figure.6a), the local Nusselt numbers are an increasing function on the disk radius. They are weakly dependent on the rotational Reynolds number for small radii ($r/D \le 4$). Near the impingement zone, the Nusselt number has two peaks. The two peaks are simultaneously at $r/D = 5$ and $r/D = 6.5$. This significant increase in heat transfer can be explained by an increase in radial velocities in the boundary layer linked to the rotor. This induces higher shear stresses near the rotating disk and consequently an increase in the local Nusselt. Moving away from the impinging point and for radii $r/D \ge 8$, the influence of rotation is noticeable by an increase in Nusselt numbers as a function of r and Re_w. A decrease in radial flow near the stator and an increase in the radial velocity gradient near the rotor induces higher tangential shear stresses near the rotor resulting in an increase in heat exchange in this area.

For a rotational Reynolds number fixed at $Re_\omega = 5.44\times10^5$ and different values of $Re_j = 16.5\times10^3$ to 49.5×10^3 (Figure.6.(b)), local Nusselt numbers are an increasing function of the air jet. The injected air flow has no noticeable influenced on local convective transfer for small radii ($r/D \le 4$) and also towards the periphery of the rotating disk ($r/D \ge 8$). However, near the impingement region and for r/D between 4 and 8, the effect of the air flow is very high and generates an area of high heat transfer manifests as peaks whose amplitude varies according to the jet Reynolds number Re_j. Three areas are then identified, separated by characteristic radii. A mixed zone with low radii ($r/D \le 4$) where heat transfers are weakly influenced by rotation and air flow. An area near the impinging point where heat transfers are dominated by the injected air flow and finally an area at the periphery dominated by rotation.

The numerical results obtained by the RSM turbulence model are in agreement with the experimental results. The average relative deviations obtained remain within the margin of error of the experimental measurements with a deviation of less than 7%. Taking into account the accuracy of the experimental results, the CFD model can be concluded to accurately predict the behaviour of convective heat exchange on the rotor surface.

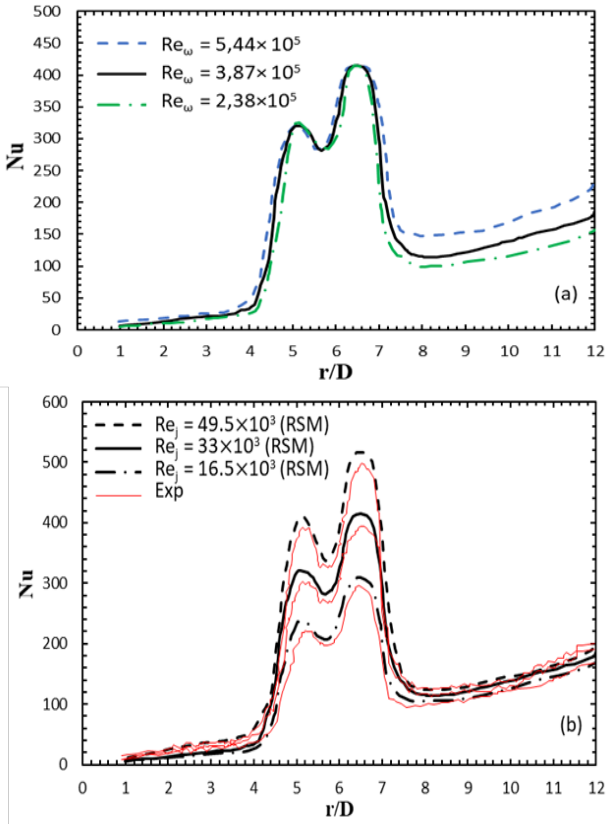

Fig.6. Distribution of local Nusselt Numbers for (a) $Re_j = 33\times10^3$, (b) $Re_\omega = 5.44\times10^5$.

Figure 7 shows the evolution of the mean Nusselt number as a function of Re_w for different values of Re_j. In this graph, the results obtained by pellé [24] in the case of a rotor-stator system without jet and simultaneously the experimental values of Boutarfa [30] corresponding to a rotating disk placed facing a parallel stator with a central opening in the stator have been shown.

Numerically, the mean Nusselt number is an increasing function of the rotational Reynolds number Re_w and the jet Reynolds number Re_j, which is consistent with the experimental results.

The numerical values of the mean Nusselt number are higher than those obtained by Boutarfa [30] and Pellé [24]. Indeed, the presence of an injected air flow requires air renewal in the air gap and cooling has become more important than in the case without a jet. The increase of the injected air flow is resulting in an increase of convective transfers on the rotor surface.

For the jet Reynolds number fixed at $Re_j = 33\times10^3$, the comparison of the numerical and experimental results shows a satisfactory agreement with using the RSM type turbulence model.

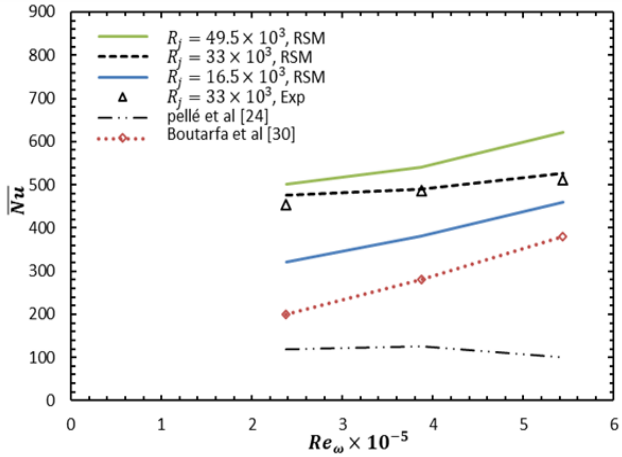

Fig. 7. Comparison of numerical and experimental results obtained in this study with those of Pellé [24] and Boutarfa [30].

5. Conclusion

This work has studied numerically and experimentally the heat transfers at the surface of a rotating disk with an eccentric impinging jet in a rotor-stator system with dimensionless spacing G = 0.02. The influence of injected air flow has been highlighted by observing the local and mean Nusselt numbers and the flow structure occurring in the air gap for different values of Re_w and Re_j.

The air jet injected giving a higher heat transfer than without the jet. The heat transfer depends on the rotational Reynolds number which, in this study, varies from 2.38×10^5 to 5.44×10^5. It also depends on the jet Reynolds number between 16.5×10^3 and 49.5×10^3. The analysis of these results identified three zones: a jet-dominated zone near the impinging jet, a mixed zone with low radii where heat transfers are slightly influenced by both the injected air flow and the rotational velocity; and finally, a zone near the periphery of the rotor where the jet influence is reduced in favor of rotational velocity.

An analysis of the radial and tangential component profiles of the air velocity in the air gap reveals that the flow is centripetal at the low radii of the air gap. The transition from an essentially centrifugal structure throughout the air gap to a centrifugal flow along the rotor and centripetal flow along the stator is carried out at large radii as the injected air flow and rotation increase.

A comparison of the local and mean Nusselt number profiles on the rotating disk surface showed that the numerical results obtained by using RSM turbulence model are in good agreement with the experimental results. The average relative deviations obtained stay within the error margin of the experimental measurements at a deviation of less than 7%.

This research work, which is part of a perspective to improving the cooling of the rotor, is currently being carried out by investigating the influence of other dimensionless spacings on convective heat transfer in the air gap between the rotor and stator.

References

[1] V. O. Okinda and N. A. Odero, "Modeling, Simulation and Optimal Sizing of a Hybrid Wind, Solar PV Power System in Northern Kenya," *Int. J. Renew. Energy Res.*, vol. 6, no. 4, pp. 1199–1211, 2016.

[2] O. Nakagoe, Y. Furukawa, S. Tanabe, Y. Sugai, and R. Narikiyo, "Hydrogen production from steam reforming of woody biomass with cobalt catalyst," in IEEE *2012 International Conference on Renewable Energy Research and Applications (ICRERA)*, Nagasaki, Japan, pp. 1-4, 11-14 Nov 2012.

[3] V. S. Fuentes, C. Troya, G. Moreno, and J. Molina, "Airfoil Selection Methodology for Small Wind Turbines," *Int. J. Renew. Energy Res.*, vol. 6, no. 4, pp. 1410–1415, 2016.

[4] P. Mazidi, G. N. Baltas, M. Eliassi, and P. Rodríguez, "A Model for Flexibility Analysis of RESS with Electric Energy Storage and Reserve," in *IEEE 7th International Conference on Renewable Energy Research and Applications (ICRERA)*, Paris, France, pp. 1004–1009,14-17 Oct 2018.

[5] A. S. Ali, M. M. Ali, A.-R. Youssef, and G. T. Abdel-Jaber, "Comparative Study of Different Pitch Angle Control Strategies for DFIG Based on Wind Energy Conversion System," *Int. J. Renew. Energy Res.*, vol. 9, no. 1, pp. 157–163, 2019.

[6] J.-S. Bae, D.-G. Choi, S.-Y. Lee, C. Yoo, and D. Kim, "Preliminary study on a fabric-covered wind turbine blade," in *IEEE 4th International Conference on Renewable Energy Research and Applications (ICRERA)*,Palermo,Italy, pp. 1196–1200,22-25 Nov 2015.

[7] M. Quraan, Q. Farhat, and M. Bornat, "A new control scheme of back-to-back converter for wind energy technology," in *IEEE 6th International Conference on Renewable Energy Research and Applications (ICRERA)*,San Dieco,CA, pp. 354–358,5-8 Dec 2017.

[8] S. Goldstein, "On the Resistance to the Rotation of a Disc Immersed in a Fluid," in *Proc.cambridge Phil .Soc*, vol. 31, no. 2,1935, pp. 232–241.

[9] E. C. Cobb and O. A. Saunders, "Heat transfer from a rotating disk," *Proc. R. Soc. Lond. A*, vol. 236, no. 1206, pp. 343–351, 1956.

[10] L. A. Dorfman, "Hydrodynamic resistance and heat loss of rotating solids, Oliver and Boyd, Edinburgh and London, 1963.

[11] M. Angioletti, R. M. Di Tommaso, E. Nino, and G. Ruocco, "Simultaneous visualization of flow field and evaluation of local heat transfer by transitional impinging jets," *Int. J. Heat Mass Transf.*, vol. 46, pp. 1703–1713, 2003.

[12] Y.-M. Chen, W.-T. Lee, and S.-J. Wu, "Heat (mass) transfer between an impinging jet and a rotating disk," *Heat mass Transf.*, vol. 34, no. 2–3, pp. 195–201, 1998.

[13] J. M. Owen and R. H. Rogers, "Flow and heat transfer in rotating-disc systems," Rotor–stator Systems, vol. 1, Research Studies Press,Taunton, UK and John Wiley, 1989.

[14] C. O. Popiel and L. Boguslawski, "Local heat transfer coefficients on the rotating disk in still air," *Int. J. Heat Mass Transf.*, vol. 18, pp. 167–170, 2005.

[15] G. K. Batchelor, "Note on a class of solutions of the Navier-Stokes equations representing steady rotationally-symmetric flow," *Q. J. Mech. Appl. Math.*, vol. 4, no. 1, pp. 29–41, 1951.

[16] K. Stewartson, "On the flow between two rotating coaxial disks," in *Mathematical Proceedings of the Cambridge Philosophical Society*, 1953, vol. 49, no. 2, pp. 333–341.

[17] J. W. Daily and R. E. Nece, "Chamber dimension effects on induced flow and frictional resistance of enclosed rotating disks," *J. basic Eng.*, vol. 82, no. 1, pp. 217–230, 1960.

[18] J. Pellé and S. Harmand, "Heat transfer study in a rotor–stator system air-gap with an axial inflow," *Appl. Therm. Eng.*, vol. 29, no. 8–9, pp. 1532–1543, 2009.

[19] T. D. Nguyen, J. Pellé, S. Harmand, and S. Poncet, "PIV measurements of an air jet impinging on an open rotor-stator system," *Exp. Fluids*, vol. 53, no. 2, pp. 401–412, 2012.

[20] S. Poncet *et al.*, "Turbulent impinging jet flow into an unshrouded rotor–stator system: Hydrodynamics and heat transfer," *Int. J. Heat Fluid Flow*, vol. 44, pp. 719–734, 2013.

[21] D. Lytle and B. W. Webb, "Air jet impingement heat transfer at low nozzle-plate spacings," *Int. J. Heat Mass Transf.*, vol. 37, no. 12, pp. 1687–1697, 1994.

[22] J. Pellé and S. Harmand, "Heat transfer measurements in an opened rotor–stator system air-gap," *Exp. Therm. fluid Sci.*, vol. 31, no. 3, pp. 165–180, 2007.

[23]G. Ritoux, "Evaluation numérique des facteurs de forme," *Rev. Phys. appliquée*, vol. 17, no. 8, pp. 503–515, 1982.

[24] J. Pellé, "Etude expérimentale des échanges convectifs sur le rotor d'une machine discoïde: influence d'un jet impactant." Valenciennes, 2006.

[25] A. Fluent, "12.0 Theory Guide," *Ansys Inc*, vol. 5, no. 5, 2009.

[26] A. Zeghib, "Comparaison des différents modèles de turbulence d'un écoulement aérodynamique dans un cyclone," 2008.

[27] M. M. Gibson and B. E. Launder, "Ground effects on pressure fluctuations in the atmospheric boundary layer," *J. Fluid Mech.*, vol. 86, no. 3, pp. 491–511, 1978.

[28] J. P. Van Doormaal and G. D. Raithby, "Enhancements of the SIMPLE method for predicting incompressible fluid flows," *Numer. heat Transf.*, vol. 7, no. 2, pp. 147–163, 1984.

[29] S. Patankar, *Numerical heat transfer and fluid flow*. CRC press, 1980.

[30] R. Boutarfa and S. Harmand, "Local convective heat transfer for laminar and turbulent flow in a rotor-stator system," *Exp. Fluids*, vol. 38, no. 2, pp. 209–221, 2005.